Chapter 4

UNCERTAINTY IN EDDY COVARIANCE FLUX ESTIMATES RESULTING FROM SPECTRAL ATTENUATION

W. J. Massman
wmassman@fs.fed.us

R. Clement

Abstract

Surface exchange fluxes measured by eddy covariance tend to be underestimated as a result of limitations in sensor design, signal processing methods, and finite flux-averaging periods. But, careful system design, modern instrumentation, and appropriate data processing algorithms can minimize these losses, which, if not too large, can be estimated and corrected using any of several different approaches. However, no flux-correction method is perfect so methodological uncertainties are inevitable. This study addresses the uncertainties in surface flux measurements that have been corrected for spectral attenuation with the transfer function approach. The sources of the errors in the estimates of flux attenuation examined here include the (flux-averaging) period-to-period variablity of cospectra, the departure of real cospectra from presumed smooth curves, the inherent variability in maximum frequency (f_x) of the frequency weighted cospectra, and possible imprecision in instrument related time constants. A method is proposed to estimate the uncertainty resulting from combining these effects. Also included in this study are a general mathematical relationship to describe spectra or cospectra, comparisons of observed cospectra for cospectral similarity, and discussions about including high-pass filters (associated with the flux-averaging procedures) when accounting for low frequency losses.

1. General issues regarding flux attenuation

Even the most carefully designed and deployed eddy covariance system will not be able to completely sample all flux-carrying turbulent atmospheric eddies. As a result, all eddy covariance systems tend to underestimate the true atmospheric fluxes. This bias results from the physical limitations in the size, separation distances, and response times of the sensors, the electronic filters used to reduce noise associated with an instrument's output signal, and the data processing algorithms intended to separate the turbulent fluctuations and their means. In general terms, the physical limitations of the instruments and any electronic filters tend to limit a system's ability to resolve the smallest eddies. Whereas, the mean-removing and flux-averaging methods resrict a system's ability to sample the largest eddies, a consequence of finite flux-averaging periods. Consequently, all eddy covariance systems are bandwidth limited and all measured fluxes are attenuated at both high and low frequencies (see Figure 4.1). No eddy covariance instrument or system is free of these shortcomings. But, by careful design and the use of modern instrumentation and electronics many of these effects can be reduced and, within reason, quantified and corrected. To date there have been several approaches developed to deal with sensor related attenuation effects. But, in most cases these approaches are variants of two broad methods: the transfer function approach and in-situ methods.

Early attempts to deal with instrument-related attenuation largely focused on developing transfer functions to describe how sonic and scalar sensor designs (sensor separation lengths and geometrical shapes) might affect the high frequency portion of spectra and cospectra measured with these instruments (e. g., Gurvich 1962; Kaimal et al. 1968; Silverman 1968; Wyngaard 1971; Hicks 1972; Horst 1973). In general, transfer functions, such as those just cited, have been developed from knowledge of atmospheric turbulence and the technology and physical principles underlying the operation of the instrumentation. However, sometimes they are also empirically determined, as Laubach and Teichmann (1996) did for water vapor tube sorption effects. By comprehensively applying spectral transfer functions to a collection of fast response instruments Moore (1986) initiated the transfer function method for estimating spectral loss associated with eddy covariance systems. More recently Horst (1997, 2000) and Massman (2000, 2001) have extended Moore's (1986) approach by expanding it to include transfer functions appropriate to newer instrumentation (e. g., Massman 1991) and by including low frequency attenuation associated with flux sampling and averaging procedures (e. g., Kaimal et al. 1989; Rannik and Vesala 1999; Rannik 2001).

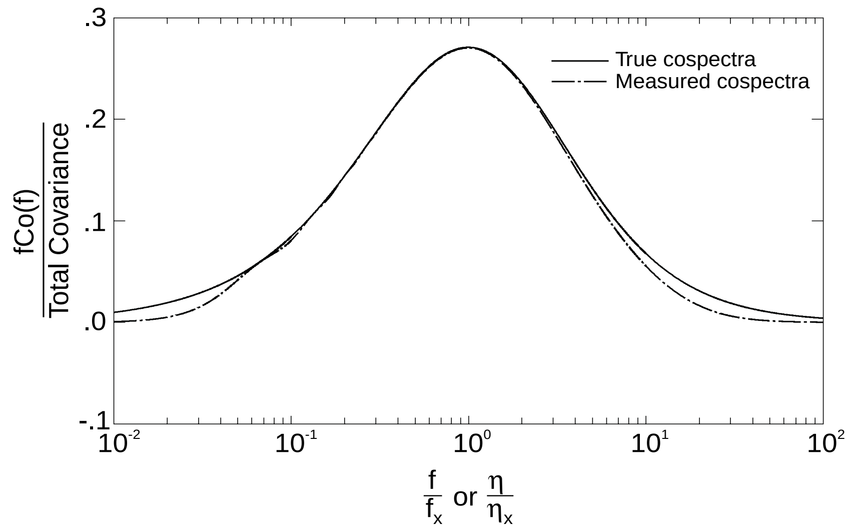

Figure 4.1. A comparison of a hypothetical frequency-weighted atmospheric cospectrum (solid line) with one measured by an eddy covariance system (dash-dot). The cospectral attenuation at high frequencies is a result of sensor line averaging, separation, and response times. The low frequency loss is a consequence of the block averaging associated with calculating time averaged fluxes. The total flux loss is related to the difference in the areas under each of the cospectral curves. Here f is frequency, f_x is the frequency at which $fCo(f)$ reaches its maximum value, and η and η_x are their respective nondimensionalized forms. Further discussions can be found in sections 2.1 and 3.2.

The transfer function method, useful as a aid in minimizing and recovering flux loss related to the design of eddy covariance systems and their data handling and flux-processing algorithms, can be summarized by the following equation:

$$\frac{(\overline{w'\beta'})_m}{\overline{w'\beta'}} = \frac{\int_0^\infty \left[1 - \frac{\sin^2(\pi f T_b)}{(\pi f T_b)^2}\right] H(f) Co_{w\beta}(f) df}{\int_0^\infty Co_{w\beta}(f) df} \tag{4.1}$$

where w' and β' are the fluctuations of vertical velocity and either the horizontal wind speed or scalar concentration; $(\overline{w'\beta'})_m$ is the measured covariance and $(\overline{w'\beta'})$ is the true or unattenuated flux; f is frequency; $H(f) = \prod_{i=1}^{N} H_i(f)$ is the product of all the appropriate transfer functions associated with high frequency attenuation; $Co_{w\beta}(f)$ is the one-sided cospectrum; T_b is the block averaging period; and $[1 - \sin^2(\pi f T_b)/(\pi f T_b)^2]$ is the transfer function associated with block-averaging. This last transfer function or filter accounts for the low frequency spectral attenuation (Figure 4.1) and, as mentioned previously, is a consequence of the need to use a finite flux averaging period and the specific method used to separate the turbulent fluctuations from their mean.

The advantages of the transfer function method are that it is fairly comprehensive, it is independent of any measured fluxes, and it can be reasonably accurate (Laubach and McNaughton 1999). All that is required to use this method are the flux averaging period, the transfer functions, and a model of the cospectra. Unfortunately, the need for a cospectral model is also a weakness of the transfer function method. Usually the cospectra are modeled as relatively smooth (continuous) functions. For example, Moore (1986) used Kaimal's et al. (1972) smooth flat terrain spectra and cospectra and Horst (2000) used a much simpler formulation for the cospectra that provided a very good approximation to the flat terrain cospectra. But, smooth spectra and cospectra are not typical of the atmospheric surface layer. In fact, virtually all observed half hourly cospectra display significant variablity and virtually none of them resemble a smooth shape (e. g., Laubach and McNaughton 1999).

Another shortcoming with the transfer function method is that it is mathematically complicated and therefore numerically intensive. Although modern PCs have alleviated this problem somewhat, still some of the transfer functions are difficult to evaluate in their original formulations and the numerical techniques required to do the integration are not necessarily obvious. Moore (1986) suggested approximating the transfer functions by simpler functions, but retained the computational aspects of Equation 4.1. Horst (1997) and Massman (2000), on the other hand, have suggested a much simpler analytical approach as an alternative to the direct use of Equation 4.1. For relatively small (high frequency) attenuation effects the analytical model is an extremely good substitute for Equation 4.1 (Massman 2000, 2001). But for relatively larger amounts of (high frequency) attenuation, Massman (2000, 2001) indicates that the analytical method can significantly underestimate Equation 4.1.

A final concern with the transfer function method is that the associated correction factors can become quite large (e. g., Villalobos 1996). This is particularly true at night or during low wind speeds (Massman 2001). Although it is less clear how significant a large correction factor, one greater than about 1.5 for example, may have on the long-term carbon budget because they are typically associated with small fluxes (Massman and Lee 2002).

Unlike the transfer function approach, in situ methods do not require smooth models of atmospheric cospectra. Fundamental to these methods is the assumption of cospectral similarity between scalar fluxes. Application of this method, in the most general terms, requires taking the ratio of a reference flux (usually assumed to have no attenuation) to an attenuated reference flux. This ratio is then used as a correction factor for a measured and cospectrally similar scalar flux. This basic approach has several variants. The pass band covariance approach, first proposed by Hicks and McMillen (1988), basically assumes cospectral similarity in the central portion of any measured scalar cospectra and that this central cospectral band is not significantly influenced by either low or high frequency attenuation effects. This approach has been used in several different ways to reconstruct or correct measured fluxes (e. g., Mestayer et al. 1990; Verma et al. 1992; Horst et al. 1997; Aubinet et al. 2001). A second variant is based on using the heat flux as both the reference flux and the degraded reference flux. This approach has been used by, among others, by Koprov et al. (1973), Lee and Black (1994), Kristensen et al. (1997), Laubach and McNaughton (1999), and Villalobos (2001) to study and correct for attenuation resulting from lateral sensor separation effects. However, Goulden et al. (1997), using a recursive low pass digital filter, applied the degraded heat flux approach for real time correction of CO_2 fluxes measured with a closed-path sensor.

While these in situ methods do not suffer from issues regarding modeled cospectra like the transfer function approach does, they, nevertheless, have drawbacks that introduce uncertainty into the fluxes when they are used to estimate flux corrections. First, cospectral similarity is not guaranteed (e. g., Katul and Hsieh 1999). Differing distributions for the sources and sinks of CO_2, H_2O, and heat will produce cospectral dissimilarity between these scalars. Second this method does not include any high frequency corrections to the reference flux, which is usually taken to be the heat flux as measured by sonic anemometry, or for line averaging effects on the vertical velocity signal. These will result in the underestimation of the corrected fluxes. However, this should be a relatively small amount (e. g., 2-6%, Massman 2001) that will likely vary with wind speed and atmospheric stability. Third, the reference flux must be large enough to be adequately resolved by the eddy covariance system; otherwise it cannot be used to define the correction factor. This often makes nighttime flux corrections problematic. (Of course flux measurement at night is difficult for other reasons as well.) Fourth, calibrating the in situ method (appropriate to closed path eddy covariance systems) is, by its nature, somewhat imprecise. For example, in order to digitally degrade the temperature flux so that it will emulate the attenuation associated with a closed-path CO_2 system, it is necessary to provide an appropriate time constant. How this time constant is determined is critical to this method. If the time constant is found by comparing spectra of temperature and CO_2 or some other trace gas, then attenuation effects resulting from any spatial separation between the CO_2 intake tube and the sonic anemometer will have to be treated separately. Furthermore, digitally degrading the temperature flux using this time constant will also introduce a phase between the sonic signal and the degraded temperature signal, which may be different than the phase between the sonic signal and the CO_2 signal. Depending on the nature of these two different phase shifts, this could result in either overestimating or underestimating the high frequency spectral correction factor for CO_2 flux. On the other hand, if this time constant is determined by comparing the observed scalar cospectra, then in principle the time constant can be influenced by any effects associated with the lateral and longitudinal separations between the CO_2 intake tube, the temperature sensor, and the sonic anemometer. Therefore, empirically determined time constants, often used to characterize closed path eddy covariance systems, can be a source of uncertainty for spectral corrections. This is much less of an issue with open path systems for which the time constants are much better defined. Fifth, low frequency corrections are not included with in situ methods, which may or may not be a serious problem because the low frequency corrections are likely to need special treatment, as discussed again in a later section.

In summary any method used for quantifying and correcting eddy covariance fluxes for spectral loss will also carry some inherent uncertainty. Such methods must employ simplifying assumptions, which will be violated to varying degrees from one eddy covariance system or instrument to another and from one flux sampling period to another. Nevertheless without such assumptions quantifying and compensating for spectral loss in eddy covariance flux data becomes prohibitive or impossible. It is, therefore, beneficial to examine the uncertainties associated with these assumptions and, if possible, to quantify them.

Specifically, this study develops a simple expression (or method) for estimating the uncertainty in the spectral correction factors derived from the transfer function method. This expression, based on Massman's (2000, 2001) analytical model for spectral corrections, includes the major aspects of cospectral variability. We focus on the transfer function method because it lends itself to error estimation more easily than does the in situ method. Nevertheless, the uncertainty analysis is also applied to a hypothetical closed path system with an empirically determined time constant. We also examine some aspects of cospectral similarity by introducing and using a general mathematical form for (ideal) spectra and cospectra and comparing heat and momentum cospectra at an AmeriFlux and a Euroflux site. Ultimately, we hope this study will provide an extended example of how to develop and assess spectral correction factors that can be used at any site and with any eddy covariance system. The next section uses a formal error analysis to define the sources of uncertainties associated with the transfer function method for estimating spectral corrections. The third section describes how the uncertainty analysis is applied to observed data.

2. Sources of uncertainties for the transfer function method

For the sake of consistency and to emphasize the relationship with Massman's (2000, 2001) approach for spectral corrections we will, as appropriate, employ his notation throughout this study. We will also henceforth reference his papers as M21.

For spectral correction methods based on transfer functions the major source of uncertainty is the variability in the cospectra from one flux averaging period to another. This cospectral variation has three aspects: (*i*) variability in the frequency, f_x, at which the frequency-weighted cospectra, $fCo(f)$, reaches a maximum value, (*ii*) variations in how relatively broad or peaked $fCo(f)$ might be (Horst 1997; M21), and (*iii*) departures of any observed cospectra during an averaging period from the assumed smooth shape. A fourth, but less significant, source of uncertainty results from (*iv*) uncertainties in an eddy covariance system's time constants. Issues (*i*), (*ii*), and (*iv*) are treated within the analytic framework developed by M21. The third concern is treated numerically. The next subsection defines the concepts related to (*i*) and (*ii*) in terms of a universal mathematical expression for cospectra and spectra. After that section 2.2 develops an uncertainty analysis using M21's analytical model. Later sections discuss closed path systems and the associated uncertainties in system time constants and also describe how the analytical results are generalized to include the issues related to (*iii*).

2.1 A general mathematical expression for spectra and cospectra

A fairly general (smooth) mathematical expression or model of cospectra that will be used with transfer function based methods to estimate spectral correction factors is

$$fCo(f) = A_0 \frac{f/f_x}{[1 + m(f/f_x)^{2\mu}]^{\frac{1}{2\mu}(\frac{m+1}{m})}} \tag{4.2}$$

where f is frequency (Hz), A_0 is a normalization parameter (discussed in more detail below), m is the (inertial subrange) slope parameter, and μ is the broadness parameter. To describe cospectra, which are normally

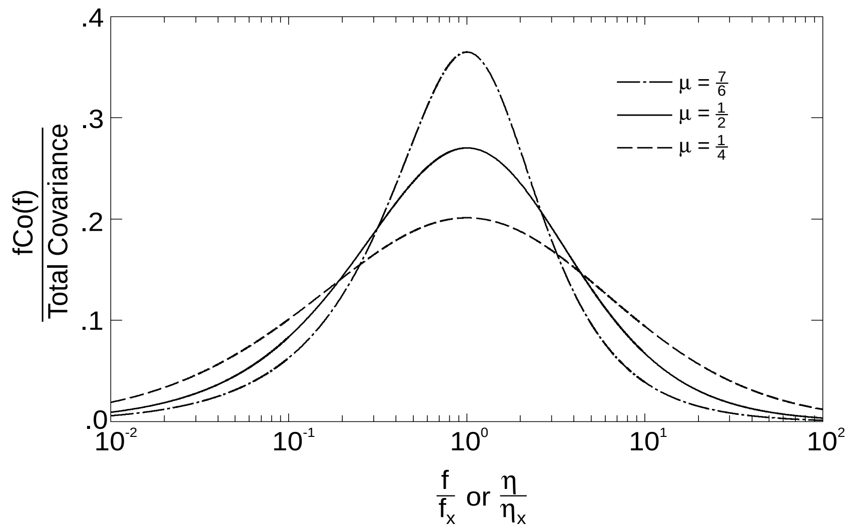

Figure 4.2. Influence of the broadness parameter μ on the shape of the cospectra modeled by Equation 4.1. For $\mu = 7/6$ Equation 4.1 approximates the flat terrain stable-atmosphere cospectra of Kaimal et al. (1972). For $\mu = 1/2$ it approximates their cospectra for an unstable atmosphere. All cospectra obey a -7/3 power law in the inertial subrange.

characterized by a -7/3 power law in the inertial subrange, m must be 3/4. To describe spectra $m = 3/2$ results in a -5/3 power law.

Equation 4.2 is a generalization of the models of spectra and cospectra discussed by Busch (1973) and Kristensen et al. (1997). It can be used to describe either normalized or unnormalized spectra or cospectra. A normalized spectra or cospectra would have unit area, i. e., $\int_0^\infty Co(f)df/(totalcovariance) = 1$. Otherwise the area under $Co(f)$ would be the total covariance. Clearly, it is possible to employ the normalization condition to eliminate A_0 from Equation 4.2. For example, the condition of unit area for a normalized spectra or cospectra yields

$$A_0 \frac{B(\frac{1}{2\mu}, \frac{1}{2\mu m})}{2\mu(m^{1/2\mu})} = 1$$

where $B(x, y)$ is the complete beta function (e. g., Spanier and Oldham 1987). However, for the present study A_0 will be taken as a free parameter. This is done largely for ease of computation, otherwise obtaining the parameters f_x, μ, and m by nonlinear regression on observed cospectra would be considerably more complicated both mathematically and numerically.

An example of the broadness parameter is shown in Figure 4.2. For $m = 3/4$ and $\mu = 7/6$ Equation 4.2 closely approximates the flat terrain stable-atmosphere frequency-weighted cospectra of Kaimal et al. (1972); whereas, for $\mu = 1/2$ it approximates their cospectral model of an unstable atmosphere. In general, Figure 4.2 shows that relatively narrow or peaked cospectra are associated with larger values of μ and that relatively broad cospectra are associated with smaller values of μ.

2.2 Analytical expression for estimating uncertainty

One of the benefits of any analytical model is that it can be used in a formal error analysis to estimate model uncertainty resulting from errors or uncertainties associated with the model's parameters. M21 shares this advantage. In it's simplest form his model yields the following expression for the ratio of the measured covariance, $(\overline{w'\beta'})_m$, to the true or spectrally unattenuated covariance, $(\overline{w'\beta'})$:

$$\frac{(\overline{w'\beta'})_m}{\overline{w'\beta'}} = [\frac{b^\alpha}{(b^\alpha + 1)}][\frac{b^\alpha}{(b^\alpha + p^\alpha)}][\frac{1}{p^\alpha + 1}] \tag{4.3}$$

where $b = 2\pi f_x \tau_b$ and $\tau_b =$ the equivalent time constant associated with block averaging (Massman 2000); $p = 2\pi f_x \tau_e$ and $\tau_e =$ the equivalent time constant associated with all high frequency attenuation (Massman 2000); and α is the broadness parameter for M21's analytical model. [Note that α is really an adjustment factor to M21's analytical model that improves the quality of the correction factor for relatively broader cospectra. It is not the same as μ, but it is related to μ and is associated with cospectra for which $\mu \leq 0.5$.] This expression assumes that recursive filtering is not used when separating the mean and fluctuating quantities so that the 'a' term of Massman (2000) is not necessary (Massman 2001).

It is useful for the present study to simplify Equation 4.3, which can be done by noting that for most applications the flux averaging period far exceeds the time constants associated with high frequency attenuation effects, i. e., $\tau_b >> \tau_e$. This allows the middle term on the right hand side of Equation 4.3 to be approximated by unity, i. e., $[\frac{b^\alpha}{(b^\alpha+p^\alpha)}] \approx 1$. The resulting correction factor, F, is the inverse of the simplified Equation 4.3 and is given next.

$$F = \frac{\overline{w'\beta'}}{(\overline{w'\beta'})_m} = [1 + \frac{1}{(2\pi f_x \tau_b)^\alpha}][1 + (2\pi f_x \tau_e)^\alpha] \tag{4.4}$$

This expression can be used to evaluate the expected error, ΔF, in the correction factor, F, resulting from period to period cospectral variations in f_x and α and from uncertainties in τ_e. Following Scarborough (1966) or Coleman and Steele (1999) the expected error is defined as

$$\Delta F = \sqrt{\left[\frac{\partial F}{\partial f_x}\Delta f_x\right]^2 + \left[\frac{\partial F}{\partial \alpha}\Delta \alpha\right]^2 + \left[\frac{\partial F}{\partial \tau_e}\Delta \tau_e\right]^2} \tag{4.5}$$

where Δf_x and $\Delta\alpha$ are the uncertainties associated with f_x and α and $\Delta\tau_e$ is the uncertainty associated with τ_e. Usually τ_b is known with sufficient precision that there is no need to include any associated uncertainty. The uncertainties associated with f_x and α can be evaluated from data, as outlined in the next section. $\Delta\tau_e$ is considered only for the closed path system, which is also discussed later. For an open path system $\Delta\tau_e$ is considered negligible. [Note that the use of τ_e in M21's model for spectral corrections does introduce some uncertainties into the spectral estimates; however they result more from mathematical approximations than from random variations. Consequently, these uncertainties are likely to produce biases (underestimations) of the true spectral correction.] Using Equation 4.4 to evaluate the partial derivatives and then setting the parameter $\alpha = 1$ in the resulting expression yields the following expression for the relative uncertainty in the correction factor, $\Delta F/F$:

$$\begin{aligned} \frac{\Delta F}{F} = \{[(1+\frac{1}{b})p - \frac{1+p}{b}]^2[\frac{\Delta f_x}{f_x}]^2 \\ +[(1+\frac{1}{b})p\ln(p) - \frac{1+p}{b}\ln(b)]^2[\Delta\alpha]^2 \\ +[(1+\frac{1}{b})p]^2[\frac{\Delta\tau_e}{\tau_e}]^2\}^{0.5}/[(1+p)(1+\frac{1}{b})] \end{aligned} \tag{4.6}$$

The broadness parameter, α, was set to 1 in this expression because its observed range variation, as discussed later, is not very great so that explicitly including it in Equation 4.6 is not necessary and because we wish to keep this expression as simple as possible.

Equation 4.6 can be interpreted in two ways. First, as previously emphasized, this expression defines the relative uncertainty in the spectral correction factor, F, used with some eddy covariance systems. However, and maybe more importantly, its second interpretation is that it also represents the uncertainty in flux estimates that use transfer function based methods to spectrally correct the measured covariances. This second interpretation follows from the fact that the correction factors are applied by multiplying the measured covariance by F. Nevertheless, this second interpretation is broader and more inclusive than what might be inferred from the assumptions underpinning its derivation. As discussed below Equation 4.6 is fairly robust and can be generalized to include other sources of uncertainty associated with spectral correction factors. The next section discusses how the model parameters f_x, Δf_x, α, $\Delta\alpha$, τ_e, and $\Delta\tau_e$ are evaluated from observed data and how Equation 4.6 is generalized and applied to the measured covariances.

3. Application of uncertainty analysis to observed data

3.1 Site description and data handling preliminaries: An AmeriFlux site

Data used in this study were obtained between January 2 and January 5, 2001 at a subalpine site within the larger Glacier Lakes Ecosystem Experiments Site (GLEES), located in the Rocky Mountains of southern Wyoming about 70 km west of Laramie, Wyoming, USA. This AmeriFlux eddy covariance site has an elevation of 3158 m and its location is (41°21′56.3″N, 106°14′22.6″W). The mean topographical slope from about 2 km upwind from the eddy covariance tower is about +3 to +5°. Beyond that the slope becomes quite steep as the land rises to a mountain peak of about 3430 m. For the purpose of measuring fluxes, the general region should be considered micrometeorologically complex. During the time of this experiment the area was snow covered. The snow depth in the clearing surrounding the eddy covariance tower was about 1.1 m and within the nearby wooded area it was about 0.7 m.

At GLEES the sonic anemometer is $z_{ref} = 27.1$ m above the ground surface and, being aligned with the dominant wind direction, is pointed nearly due west (268°). Year round the winds almost exclusively fall within the sector between 230° and 310°. This sector is forested and covered by Engelmann spruce (*Picea engelmannii* (Parry) Englem.) and subalpine fir (*Abies lasiocarpa* [Hook.] Nutt.), which range in height (h) between 15 and 20 m and in age between 250 and 450 years old. However, the region generally is patchy and also includes seasonally wet meadows, open areas within the forest, and several lakes of various sizes. During the winter months the half-hourly mean winds can vary between about 2 $\mathrm{m\,s^{-1}}$ and 25 $\mathrm{m\,s^{-1}}$, with an mean ensemble average of about 10 $\mathrm{m\,s^{-1}}$. The zero-plane displacement height, d, for this site is assumed to be 13 m (or $d \approx 0.75h$). The mean temperature is about -10 C and the mean pressure is about 69 kPa. As a result of solar heating of the trees and needles the sensible heat fluxes during the daylight can be large (∼300 $\mathrm{W\,m^{-2}}$), as can the latent heat fluxes (∼200 $\mathrm{W\,m^{-2}}$), which is driven by sublimation of the snow. CO_2 fluxes during the winter are low ($\sim$0.02 $mg\,m^{-2}s^{-1}$) and are a combination of efflux from the snow surface and from the tree boles. Clearly the source distributions for heat, CO_2, and water vapor fluxes are quite different at GLEES. In spite of the relatively high heat and vapor fluxes atmospheric stability at GLEES during the winter is assumed to be neutral during the January 2001 study period. This is because GLEES is very windy and extremely turbulent almost continuously during the winter months so that $z_{ref}/L = 0$ virtually 24 hours a day. Here L denotes the Monin-Obukhov length.

The turbulence data were obtained with an ATI sonic anemometer (thermometer), model no. SATI/3VX and an open-path NOAA ATDD infrared CO_2/H_2O sensor (Auble and Meyers 1992). Also included as part of this study is a fast response pressure sensor for measuring static turbulent pressure fluctuations (Cook and Bedard 1971; Nishiyama and Bedard 1991; Wyngaard et al. 1994), which is treated in this study as another atmospheric scalar. The sonic has a path length of 0.15 m. The open-path CO_2/H_2O sensor has a path length of 0.20 m and is mounted 0.25 m below the center of the sonic. Relative to the sonic the open-path sensor was displaced laterally by 0.051 m and longitudinally (behind the sonic) by 0.22 m. The pressure probe is connected to a differential pressure sensor by a 6.1 m long garden hose with a diameter of 0.025 m. The probe is positioned 0.33 m above the center of the sonic and has a path length of 0.045 m. It is displaced laterally by 0.051 m relative to the sonic and located 0.356 m behind the sonic.

For the purposes of the present work, we do not include any possible attenuation associated with vertical displacements (e. g., Kristensen et al. 1997) or possible tube effects on the pressure fluctuations (e. g., Aydin 1998; Iberall 1950). For the open path CO_2/H_2O instrument, which is mounted 0.25 m below the sonic, Kristensen's et al. (1997) results suggest that correction term is about +0.2%, which is negligible. However, at GLEES the pressure probe is mounted 0.33 m above the sonic. To date there are no models of covariance loss to the pressure covariance, $\overline{p'w'}$, resulting from vertical displacement. It is, therefore, possible that measured values of $\overline{p'w'}$ are underestimated because we neglect this aspect of system design. We do not include any possible influences the hose may have on the pressure fluctuations measured with the differential pressure sensor because again we expect this to be negligible (e. g., Holman 2001, Chapter 7). With these few exceptions, we use all the system design distances and the other instrument and block averaging filtering effects and Massman's (2000) analytical approach to estimate the system's equivalent time constant for high frequency, τ_e, and low frequency, τ_b, attenuation.

All GLEES turbulence data are sampled at 20 Hz and the flux averaging period is half an hour. Before any fluxes are calculated the 20 Hz data are screened for spikes using Højstrup's (1993) despiking and interpolating routine. The data are also tested for physically unrealistic values of skewness and kurtosis (Vickers and Mahrt 1997). Nevertheless, this specific period of time, consisting of 180 contiguous half hour periods, was chosen for this analysis because the data capture rate was extremely high and the data system and the data itself showed no significant problems. After despiking, the data were then used to form half-hourly mean wind speeds which are used with the planar fit method (Wilczak et al. 2001) to define the coordinate system. Next, all 20 Hz data are rotated into this coordinate system and it is this rotated high frequency turbulence data that are used for calculating cospectra. For this study the GLEES cospectral data include the momentum covariance, $\overline{u'w'}$, the pressure covariance, $\overline{p'w'}$, the sonic virtual temperature covariance, $\overline{w'T'_v}$, and the water vapor ($\overline{w'\rho'_v}$) and CO_2 ($\overline{w'c'}$) covariances. In the case of the last two covariances we do not include the WPL terms (Webb et al. 1980) because we are correcting only the covariance between the sonic and the open-path CO_2/H_2O sensor.

3.2 Observed values of the cospectral parameters f_x, Δf_x, α, and $\Delta\alpha$

After rotation there are six steps that are performed to derive estimates of f_x and Δf_x.

- Each time series is padded with about 860 zeroes to make a total of 36,864 ($N_{FFT} = 2^{12}3^2$) data points. We note here that these winter time series showed no significant temporal half-hourly trends so that padding with zeroes should cause only a minimum of distortion in the cospectra (see Chapter 7 of Kaimal and Finnigan 1994). The FFT we employed here is very general and because it can accept any number of data points it is not restricted to a power of 2. However, this FFT performs best and as fast as a standard FFT if the number of input data points is rich in powers of small primes. For a half-hour time series, sampled at 20 Hz, this value of N_{FFT} is the optimal value for FFT performance.
- After transforming the time series and forming the cospectra, the discrete cospectral estimates are corrected for the reduction associated with the padding by zeroes (Kaimal and Finnigan 1994).
- The raw cospectra are then smoothed with a frequency window that expands with frequency (Kaimal and Finnigan 1994). How-

ever, no other windowing or tapering was used on the time series or the cospectra (e. g., Kaimal and Finnigan 1994).

- The FFT frequencies, f, are nondimensionalized (multiplied) by the ratio z_{ref}/u to yield the nondimensional frequency, $\eta = f z_{ref}/u$.

- The smoothed cospectral estimates are then multiplied by frequency to form the frequency-weighted cospectra, which is fitted to the universal cospectra given by Equation 4.2 using the Levenberg-Marquardt nonlinear least squares algorithm (Press et al. 1992). We fit the frequency weighted cospectrum rather than the cospectrum itself because the frequency weighted cospectrum has more structure (i. e., it is not monotonic, which the cospectrum tends to be) so it provides a more reliable and precise estimate of the parameters. We also only fit the central portion of the observed cospectra to avoid influencing the fit by any high or low frequency attenuation. Note here that the transformation to nondimensional frequencies has no impact on Equation 4.2 or the results of the fitting procedure because $f/f_x = \eta/\eta_x$. Nor does it have any impact on the relative uncertainty in the correction factor, $\Delta F/F$ given by Equation 4.6, because $\Delta f_x/f_x = \Delta\eta_x/\eta_x$. Nevertheless, when presenting the f_x results we also include another nondimensional form for f_x, i. e., $\eta'_x = f_x(z_{ref} - d)/u$. This second formulation, which is more conventional, allows us to compare our results with those of previous studies and is used specifically in Equations 4.6 and 4.3 when parameterizing f_x. But because the displacement height, d, is somewhat uncertain, it also follows that η'_x is less certain that η_x. However, we do not include this source of uncertainty in our results.

- It is necessary to explore the parameter space in order to determine the optimal values of the parameters f_x, μ, and m, the slope parameter. Although the slope parameter is not the primary objective of the study it is useful to be able to examine the slope of the inertial subrange for its own interest as well as to assess its possible influence on the uncertainties in f_x and μ. Exploring the parameter space consists of fitting each of the cospectra several different times using different choices for the initial values of the parameters and different combinations of fixed and free parameters. The goal is to find a set of initial values for the parameters that produce the highest ensemble R^2 values (best fit to the ensemble of cospectra). This results in a set of optimized parameter values for each cospectrum. The ensemble mean and the root mean square

Table 4.1. Optimal parameter values for instrument covariances measured at GLEES in Rocky Mountains of southern Wyoming during January 2001. At this site during wintertime the atmosphere is neutrally stable. The uncertainty associated with the value of each parameter is enclosed by parentheses. Here $\eta_x = f_x z_{ref}/u$ and $\eta_x' = f_x(z_{ref} - d)/u$.

Parameter	$\overline{p'w'}$	$\overline{u'w'}$	$\overline{w'T_v'}$	$\overline{w'\rho_v'}$	$\overline{w'c'}$
μ	0.25 (0.06)	1.0 (0.35)	0.6 (0.28)	0.6 (0.28)	0.6 (0.38)
η_x	0.22 (0.09)	0.14 (0.04)	0.21 (0.06)	0.19 (0.06)	0.22 (0.09)
η_x'	0.11 (0.05)	0.07 (0.02)	0.11 (0.03)	0.10 (0.03)	0.11 (0.05)
α	0.8 (0.2)	1.0 (0.2)	1.0 (0.2)	1.0 (0.2)	1.0 (0.2)

variance of these optimized parameter values are then taken to be the final (best) values for a parameter and its inherent uncertainty or variability. For these fitting runs $m = 3/4$ is fixed. After determining the best estimates of η_x and μ, m is then varied between 0.7 and 0.8 to test the influence different m values may have on the quality of the fits. A final run is then performed where η_x, μ, and m are fit simultaneously to confirm that all parameter values are near optimal. This last run is performed primarily to confirm that $m \equiv 3/4$ (-7/3 cospectral decay) is reasonable for these cospectra.

The results of the tests concerning the slope parameter, m, confirmed that the inertial subrange decays according to -7/3 law and that no significant improvement in the quality of the fits could be achieved by another value of the -7/3 slope ($m = 3/4$). This was true for all five instrument covariances measured at GLEES.

The final values for μ, η_x, and η_x' and their associated uncertainties are listed in Table 4.1. M21's broadness parameter value is also listed in Table 4.1, but before discussing it is worthwhile comparing the present results with the results of Kaimal et al. (1972). For flat terrain and a neutral stability Kaimal et al. (1972) suggest that $\eta_x' = 0.085$ for the momentum flux, $\overline{u'w'}$, and 0.079 for the heat flux, $\overline{w'T'}$. This study indicates that the peak in the frequency weighted cospectrum is shifted to slightly lower values at GLEES for momentum flux and slightly higher values for the heat flux. But, the uncertainties are relatively large for the GLEES site, so an precise comparison is difficult.

From the formulations given by Kaimal and Finnigan (1994) for near neutral momentum cospectra, it is straightforward to obtain that the flat terrain cospectral broadness is $\mu = 1/2$. At the more topographically complex GLEES site, however, $\mu = 1$ indicating that the frequency-weighted cospectrum is more narrowly peaked than for flat terrain. For heat flux the comparison is complicated by the fact that the model cospectra presented by Kaimal and Finnigan (1994) is comprised of two equations (i. e., it is piecewise continuous). But the same general conclusion seems to hold for the broadness of heat flux cospectra as for momentum cospectra, except that the difference between the flat terrain and the GLEES heat flux cospectral broadness parameters, μ, is somewhat smaller and less significant than for the momentum broadness parameter. We conclude that, except for some subtle nuances, the momentum and heat cospectra over the forested complex terrain at GLEES are similar to the flat terrain momentum and heat cospectra. Furthermore, it is not clear how significant, if at all, these subtle differences are. This is because (*i*) Kaimal et al. (1972) did not use Equation 4.2 to describe their cospectra, (*ii*) they did not use the same coordinate system as the present study, and (*iii*) the variability we found in the GLEES cospectral parameter values suggests that Kaimal's et al. (1972) sample size may not have been adequate to determine the natural variability that was present at the time their data were obtained. Nevertheless, when using M21's analytical method to estimate the spectral correction factors appropriate to GLEES we will use the data from Table 4.1, rather than the cospectral model from Kaimal et al. (1972).

Table 4.1 also indicates that the measured water vapor and CO_2 covariance cospectra largely follow the heat covariance cospectra because without the WPL terms these covariances are dominated by the heat flux term. In fact the CO_2 covariance is probably more strongly influenced by the heat flux term than is the water vapor covariance because the true CO_2 flux is quite small, whereas the true water vapor flux can be quite high even during the winter. Therefore, the heat flux term has a relatively smaller contribution to the $\overline{w'\rho_v'}$ covariance than to the CO_2 covariance. This and the possibility of heat and vapor dissimilarity may explain why the cospectral parameter value of η_x or η_x' for water vapor differ more from the heat covariance values than do the CO_2 covariances. We also note that the uncertainties in the parameter values for the CO_2 covariance are greater than for either $\overline{w'T_v'}$ or $\overline{w'\rho_v'}$. This may be due to the fact that the CO_2 covariance combines the variability in all the other fluxes, CO_2, water vapor, and heat.

Finally, because Kaimal et al. (1972) did not measure the pressure covariance, $\overline{p'w'}$, it is not possible to compare the present results with theirs. However, Table 4.1 does indicate that the $\overline{p'w'}$ cospectra are considerably broader than $\overline{u'w'}$ cospectra. This may be a general characteristic of $\overline{p'w'}$ cospectra as Wilczak (personal communication) has found the same characteristic also occurs over the ocean.

The parameter α and its associated uncertainty, $\Delta\alpha$, are determined empirically by matching the correction factors generated by M21 analytical approach to those generated by direct integration using Equations 4.1 and 4.2. The results, shown in Table 4.1, indicate, as M21 claimed, that the analytical method is not particularly sensitive to the broadness parameter. The only possible exception to this in this study are the $\overline{p'w'}$ cospectra ($\alpha = 0.8$), which are extraordinarily broad ($\mu = 0.25$) when compared to the other cospectra ($\mu > 0.50$). M21 also found that Kaimal's et al. (1972) flat terrain cospectra for neutral or unstable atmospheric stability also showed sufficient broadness that $\alpha = 0.925$ was required for a good match. These two non-unity values of α suggest that $\Delta\alpha$ can be estimated from the observed range of variability in the different computed values for α. We, therefore, take $\Delta\alpha = 0.2$ since the observed values of α range from 0.8 to 1.0. For the purposes of estimating $\Delta F/F$ from Equation 4.6 we will take the nominal value of α as 1, as was discussed previously.

As an example of the different steps involved in this analysis, Figure 4.3 compares the three following cospectra: the smoothed FFT cospectrum for $\overline{w'T_v'}$ obtained at 6:30 am MST January 2, 2001 (dashed line), the optimal fit of the FFT cospectrum by Equation 4.2 (solid line), and the modeled cospectrum derived from Equation 4.2 using the ensemble best fit parameters given in Table 4.1 (dotted line). This figure clearly indicates the nature of the three types of cospectral variability mentioned previously.

3.3 Cospectral (dis)similarity between sites: A Euroflux site

The last section includes a brief comparison between the flat terrain (momentum and heat) cospectra of Kaimal et al. (1972) and the cospectra obtained at a topographically complex site during neutral atmospheric conditions. The results indicated that there were cospectral differences between these sites, but it was less clear how significant the differences might be for discussions of cospectral similarity. However, for spectral attenuation issues the differences are quite significant because η_x' for momentum flux was about 18% lower at GLEES than at the flat terrain site. Whereas η_x' for heat flux was almost 40% higher at GLEES. It is, therefore, worthwhile to include another site in this comparison in an effort to determine how generalizable the previous results might be from one site to another.

This section presents values of η_x' were obtained at Griffin Forest, a Euroflux site located at (56° 36' 30" N, 3° 47' 15" W) near Aberfeldy, Perthshire, Scotland. The forest at this site covers about 75% of the surface and is 97.3% Sitka spruce (*Picea sitchensis*), 2.1% Douglas fir (*Pseudotsuga menziesii*) and 0.6% birch (*Betula pendula*). The remaining 25% of the surface is open space: roads, streams, and ridges dominated by heather and grasses. The forest Leaf Area Index (LAI) is about 8, and where the canopy is closed, the understory is quite sparse and dominated by mosses. The canopy height is about 7.5 m and d averaged about 6.5 m.

The site has an elevation of 350 m ASL, and is also a micrometeorologically complex site, being located in a region of ridge and valley ranging in height between 50 and 600 m. It is situated in a broad northwest facing valley with a mean slope of 9%. The fetch to the southwest is about 500 m before it is disturbed by a hill. To the northwest the fetch is about 2000 m and to the northeast and southeast it is about 1000 m. The eddy covariance instruments are mounted at 15.5 m and consist of a Solent R2 three dimensional sonic, a closed-path Licor (6262) CO_2/H_2O Infra Red gas analyzer (IRGA), and an open-path Licor 7500 IRGA. The inlet to the closed-path IRGA is located 0.20 m below and 0.05 m to the north of the sonic. The intake tube length is 18 m and it has an inside diameter of 0.00623 m. The flow rate is 6 L min^{-1} and the flow Reynolds number is about 1400. The open-path sensor is positioned 0.30 m from the center of the sonic. Data from this Euroflux site were obtained between July and September 2000. They were collected at 20.833 Hz ($N_{1/2} = 37500$ data points per half-hour) and were processed by the Edisol/EdiRe software package. The eddy correlation system and the data processing package are described in more detail by Moncrieff et al. (1997). All covariances are calculated in the planar fit coordinate system (Wilczak et al. 2001).

All Griffin forest cospectra are calculated for each 2-hour period using smoothed and spliced FFT (Kaimal and Finnigan 1994). To obtain the high frequency portion of the cospectra the 20.833 Hz time series are divided into M sequential segments of contiguous 512-point time series. [Note that for this method of cospectral analysis $N_{FFT} = 2^9$ and $M = 4N_{1/2}/N_{FFT}$ if N_{FFT} divides $4N_{1/2}$ exactly, otherwise $M = 1+$ the integer part of $\{4N_{1/2}/N_{FFT}\}$.] If necessary, the final segment is zero-buffered to insure that N_{FFT} is the same for all M data segments. Each segment is detrended using a linear least squares fit and tapered using a Hamming window (Kaimal and Kristensen 1991). The FFT is applied to each segment and the transformed results are averaged prior to logarithmic bin-averaging of the spectral estimates. The low frequency cospectrum for the same data period is obtained by averaging M sequential data points to obtain a single set of N_{FFT} averaged data

Table 4.2. Optimal values of η'_x for instrument covariances measured at Griffin forest, Scotland, during July through September 2000. The uncertainty associated with the value of each parameter is enclosed by parentheses. Here $\eta'_x = f_x(z_{ref} - d)/u$.

Covariance	η'_x very unstable: $z/L \leq -2$	η'_x neutral stability:	η'_x stable: $z/L > 0$
$\overline{u'w'}$	0.009 (0.063)	0.027 (0.063)	0.029 (0.015)
$\overline{w'T'_a}$	0.010 (0.032)	0.073 (0.032)	0.043 (0.025)
$\overline{w'\rho'_v}$ (closed-path)	0.003 (0.008)	0.015 (0.008)	0.014 (0.011)
$\overline{w'c'}$ (closed-path)	0.011 (0.015)	0.043 (0.015)	0.041 (0.023)
$\overline{w'\rho'_v}$ (open-path)	0.014 (0.019)	0.041 (0.019)	0.036 (0.024)
$\overline{w'c'}$ (open-path)	0.009 (0.011)	0.047 (0.011)	0.040 (0.021)

points. Again this data series is detrended, tapered, transformed, and logarithmically bin-averaged using the same methods as with the high frequency portion. The resulting high and low frequency portions are merged and sorted by frequency to obtain a single cospectral curve, to which Equation 4.2 is then fitted. About 200 cospectra for both stable and neutral/unstable atmospheric conditions were available for analysis.

Table 4.2 presents the cospectral parameter values for η'_x obtained for Griffin forest. The other cospectral parameter values are not included because they are of less significance. There are several key observations concerning the Griffin forest results that need to be emphasized. First, comparing the neutral stability η'_x values with those of GLEES (Table 4.1) indicates that for neutral conditions η'_x at Griffin forest are associated with much lower frequencies than at GLEES. Second, η'_x at Griffin forest tends to decrease with increasing atmospheric instability and that η'_x for stable conditions tend to be relatively constant and highly variable. This stability dependency is opposite of the flat terrain site of Kaimal et al. (1972), where constant η'_x is associated with unstable conditions and η'_x tends to increase with increasing atmospheric stability. Third, the open-path water vapor and CO_2 covariances and the closed-path CO_2 covariance can probably be considered cospectrally similar for any atmospheric stability, especially given the uncertainty of their respective η'_x values. But, some divergence between open- and closed-path results should not be unexpected because the influence of the WPL temperature covariance (heat flux) term will be considerably greater on the open-path covariance than on the closed-path covariance. However, the closed-path water vapor cospectra are so different from these other three scalar cospectra that they are probably untrustworthy. We hypothesize that the water vapor fluctuations have been so strongly attenuated by the tube flow and interactions with the flow path walls that their associated η'_x values should not be used for spectral attenuation issues. Fourth, the $\overline{w'T'_a}$ cospectra is for the atmospheric heat flux not for the sonic temperature covariance; but, any differences introduced by using $\overline{w'T'_a}$ rather than $\overline{w'T'_v}$ should be small. Fifth, and final, no continuity requirement between stable and neutral values of η'_x was imposed. Except for $\overline{w'T'_a}$, the results suggest that the η'_x values are probably continuous across these two stability classes. Although the variability of η'_x for $\overline{w'T'_a}$ is high in both stability classes, the data suggest that the value of 0.073 for the neutral case is likely to be biased high.

In summary, the results from this Euroflux site, when combined with those from GLEES and Kaimal et al. (1972), suggest that cospectra, which use the η'_x normalization to parameterize f_x, possess considerable site-to-site variablity. Therefore, any investigation of issues involving spectral attenuation of eddy covariance data needs to be examined on a site specific basis and that the arbitrary use of Kaimal's et al. (1972) model for η'_x has the potential to introduce significant errors into spectral correction factors for eddy covariance fluxes.

Besides any possible site-to-site variability in cospectra there is also the inherent variability of cospectra from one flux-averaging period to the next.

3.4 Departures from smooth cospectral shapes

As Figure 4.3 clearly indicates observed cospectra are not particularly smooth. This departure from a smooth cospectral shape is another source of uncertainty in spectral corrections. Although obviously related to possible uncertainties in f_x and μ, this source of uncertainty is, nevertheless, different than these other two. The ideal method for spectral corrections might very well be to use the transfer function method, Equation 4.1, combined with half hourly cospectra, which would thereby include the half-hourly departures from a smooth cospectral shape. However, this will probably never be achieved, but it can be emulated by modifying the smooth cospectral shapes given by Equation 4.2 using a random number generator (Press et al. 1992) to change the smooth cospectra into a much 'nosier' cospectra than would traditionally be used. Figure 4.4 compares a smooth cospectra with a nosier cospectra produced by this method. By providing several different integer seed values (Press et al. 1992) to the random number generator and calculating the spectral correction factor with many different noisy cospectra, we quantify the affects of random variablity in the cospectra on the spec-

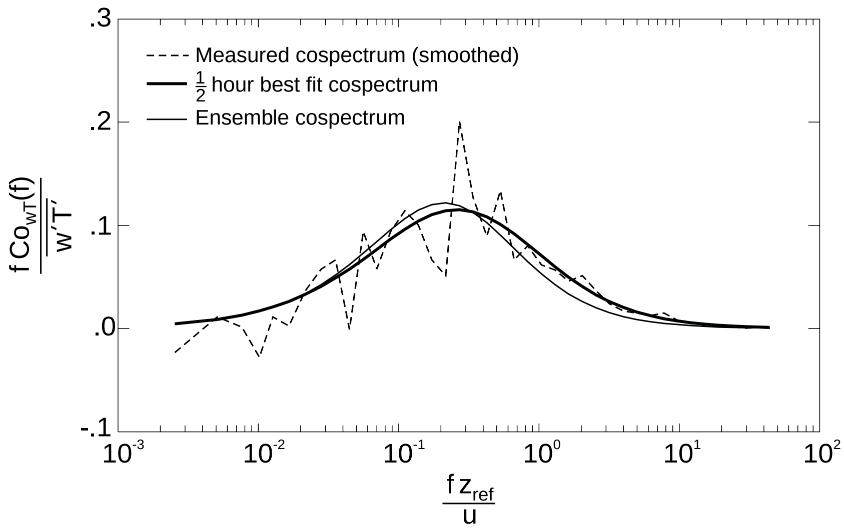

Figure 4.3. Comparison of the smoothed FFT cospectrum for $\overline{w'T_v'}$ obtained at 6:30 am MST January 2, 2001 at the GLEES (dashed line) with the optimal fit to this cospectrum with Equation 4.2 (solid line) and the modeled cospectrum derived from Equation 4.2 using the ensemble best fit parameters given in Table 4.1 (dotted line).

tral correction factor. Each of the spectral correction factors developed with a non-smooth cospectra using the integral method is compared to the correction factors determined by M21's analytical method, which uses the smooth cospectra. This produces a range of variation in F that could be conveniently incorporated into Equation 4.6 for $\Delta F/F$ by simply multiplying Equation 4.6 by a constant, $C = 1.2$. Note that the value of 1.2 was synthesized from all five of the GLEES covariance measurements. A separate determination of C for a closed path CO_2 system was also performed and is discussed in section 3.5. The final expression for the relative uncertainty, $\Delta F/F$, is

$$\begin{aligned}\frac{\Delta F}{F} &= C\{[(1+\frac{1}{b})p - \frac{1+p}{b}]^2[\frac{\Delta f_x}{f_x}]^2 \\ &+[(1+\frac{1}{b})p\ln(p) - \frac{1+p}{b}\ln(b)]^2[\Delta\alpha]^2 \\ &+[(1+\frac{1}{b})p]^2[\frac{\Delta\tau_e}{\tau_e}]^2\}^{0.5}/[(1+p)(1+\frac{1}{b})] \qquad (4.7)\end{aligned}$$

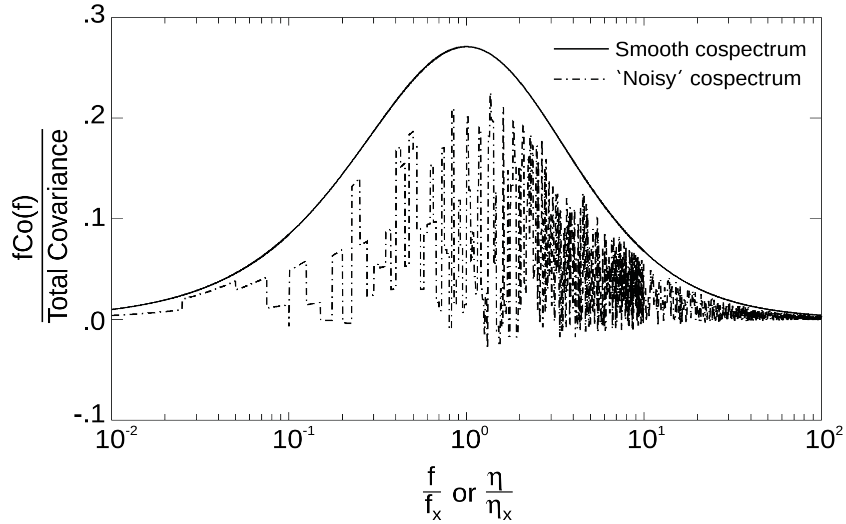

Figure 4.4. A comparison of the hypothetical frequency-weighted atmospheric cospectrum shown in Figure 4.1 (solid line) with a version of it after modification by a random number generator (dash-dot). This method of modifying the smooth cospectral shape is used to estimate the uncertainty in the spectral correction factor that is associated with departures of true cospectra from smoothed versions of the cospectra.

3.5 Results for an open-path system

Figure 4.5 shows relative uncertainty in the spectral correction factor, $\Delta F/F$, as a function of wind speed for the GLEES CO_2 covariance measurement. This figure suggests that applying a spectral correction factor based on the transfer function approach to GLEES wintertime CO_2 covariances would lead to a 5 to 10% uncertainty in the resulting CO_2 covariance at low wind speeds and a 2 to 4% uncertainty at higher wind speeds. Figure 4.6 shows the correction factor, F, as a function of wind speed for the GLEES CO_2 covariance measurement as estimated by the analytical method of M21 along its inherent range of uncertainty as predicted by Equation 4.7. The filters and equivalent time constants employed for this and the previous figure are taken from Table 1 of Massman (2000) and include sonic line averaging for scalar fluxes, lateral separation, longitudinal separation without a first order instrument, and high pass block averaging. The results shown in this figure indicate that the uncertainty associated with a relatively larger value of F is itself relatively large and that the inherent uncertainty in F decreases as F decreases. This supports the conclusion that if an eddy covariance

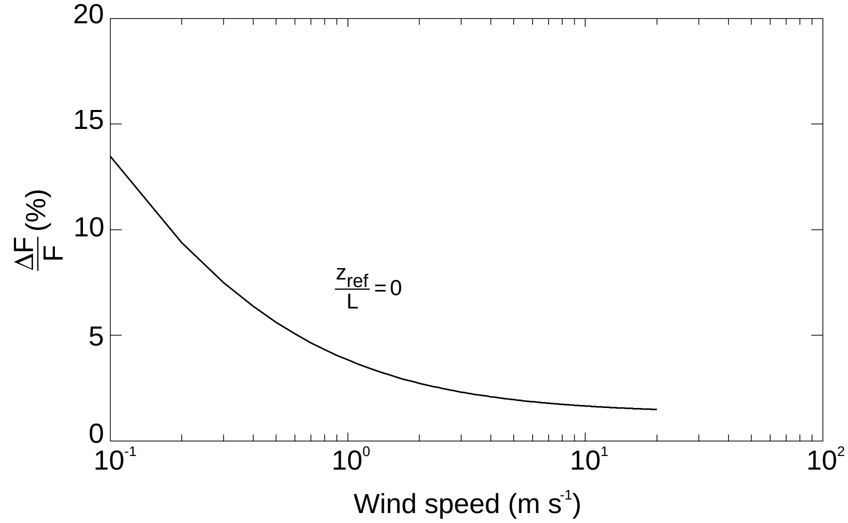

Figure 4.5. The relative uncertainty in the spectral correction factor, $\Delta F/F$, as a function of wind speed for the GLEES CO_2 covariance measurement. Neutral atmospheric stability is assumed.

system is designed so that spectral attenuation is minimal (and therefore relatively small), then the transfer method of estimating spectral correction factors is not particularly sensitive to the shape, the lack of smoothness in the cospectra, or the natural variablity of the cospectra. To rephrase, if the spectral correction factors are small, then the transfer function method should provide trustworthy and relatively accurate values for the spectral correction factors.

3.6 Extension to a closed-path system and $\Delta\tau_e$

The GLEES data provide an example of an eddy covariance system with an open path CO_2 sensor. Now we wish to examine the same system with a closed path sensor. We construct this scenario primarily to test our present methods on a system that has a much longer equivalent time constant for high frequency attenuation, τ_e, than the open path system. All the methods and calculations remain the same, except we assume that the closed path system has an intake tube attached to a first order instrument, which is housed in a separate shelter at the base of the tower. We further assume that the time constant for the first order instrument (τ_1) was determined in situ to be 0.1 s and we will take $\Delta\tau_e = 25$ % of τ_1. These values for τ_1 and $\Delta\tau_e$ are to be understood as purely hypothetical. For any real application they could depart signifi-

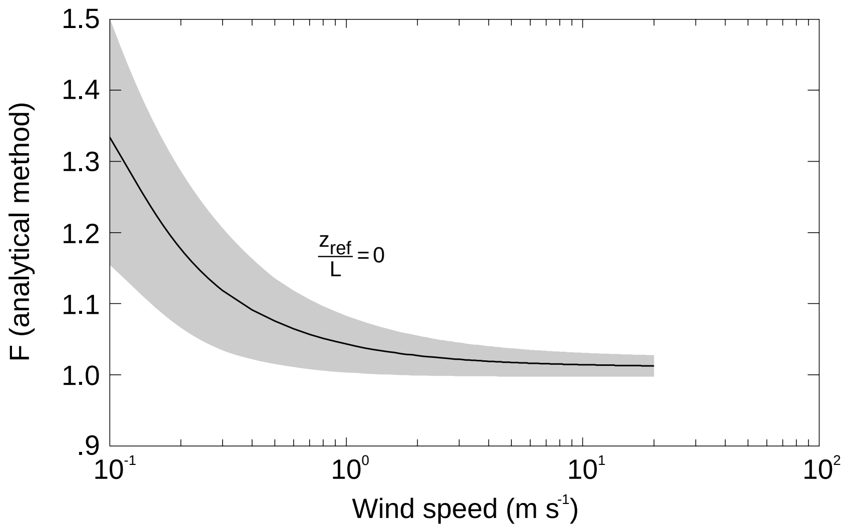

Figure 4.6. The correction factor, F, as a function of wind speed for the GLEES CO_2 covariance measurement as estimated by the analytical method of M21 (dark solid line) and its inherent range of uncertainty as predicted by Equation 4.7 (shaded area). The factor C used with Equation 4.7 to account for variable (random) departures from a smooth cospectral shape is 1.2.

cantly from these present values and from one eddy covariance system to another.

In this simulation we allow for the attenuation associated with tube flow (M21; Massman 1991), a small amount of lateral separation, some small amount of longitudinal separation with first order effects (Massman 2000), and a first order time constant for the CO_2 sensor equal to 0.1 s. Because this closed path scenario falls into M21's category for systems characterized by equivalent time constants between 0.1 and 0.3 s and a neutrally stable atmosphere, his analytical approach would suggest that Equation 4.3 above be augmented by the term $[1 + 0.9p^{\alpha}]/[1 + p^{\alpha}]$. Here we do not employ the additional term. Rather we use Equation 4.3 directly. Figure 4.7 shows the difference between the integral method, Equation 4.1, and Equation 4.3. For all wind speeds the difference is small and the agreement is quite good.

Figure 4.8 shows the correction factor, F, as a function of wind speed for the simulated closed path CO_2 covariance measurement as estimated with analytical method of M21 along its inherent range of uncertainty as predicted by Equation 4.7. For this example, the factor of C in Equation 4.7 was again found to be 1.2 using the same method as the open path sensor. This figure is the closed path analog to Figure 4.6

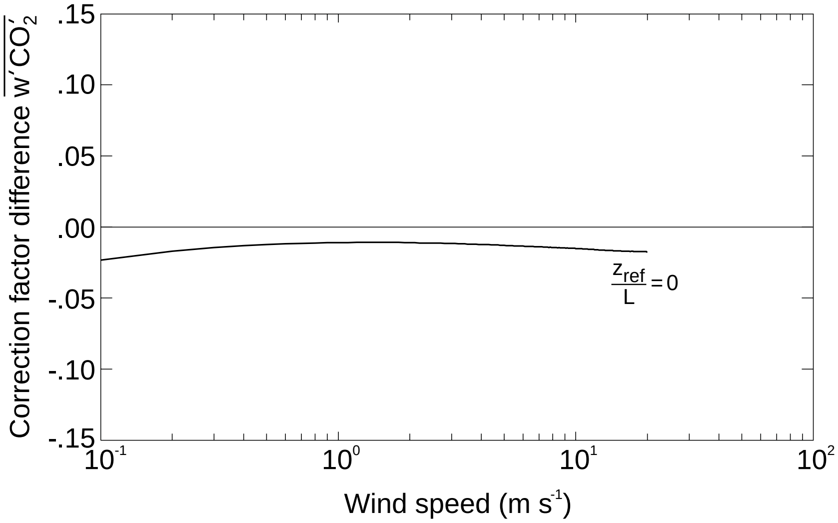

Figure 4.7. Difference between the spectral correction factors estimated from the numerical integration of Equation 4.1 and Equation 4.3 from M21. These calculations are for a closed-path eddy covariance system and a neutral atmosphere and are shown as a function of the horizontal wind speed. The zero line is highlighted.

and clearly demonstrates the same conclusions. That is if the correction factors are relatively large, which they are here by design, then the inherent uncertainties associated with the transfer function method can also be relatively large. For example the calculations shown in Figure 4.8 suggest that for wind speeds between about 2 and 10 $\mathrm{m\,s^{-1}}$ the correction factor is about $1.1 \pm 10\%$. For this same range of wind speeds Figure 4.6 suggests that the open path system has a correction factor and an inherent uncertainty about half of that. In these two examples the fundamental difference between the open and closed path systems is their respective time constants, reinforcing the notion that longer time constants result in more spectral attenuation, greater uncertainty in the spectral corrections, and, therefore, greater inherent uncertainty in the fluxes or covariances that are spectrally corrected with the transfer function method.

Most of the uncertainty shown in Figure 4.8 results from variability in the cospectra and from the uncertainty in the cospectral parameters, not from $\Delta\tau_e$. This is because the present example is fairly conservative in its estimate of τ_1 and $\Delta\tau_e$. As either of these parameters increase in value so also do the estimates for F and ΔF. At some eddy covariance sites τ_1 can exceed 1 s, which is considerably longer than the present hypothetical value of 0.1 s. At present there has been no information

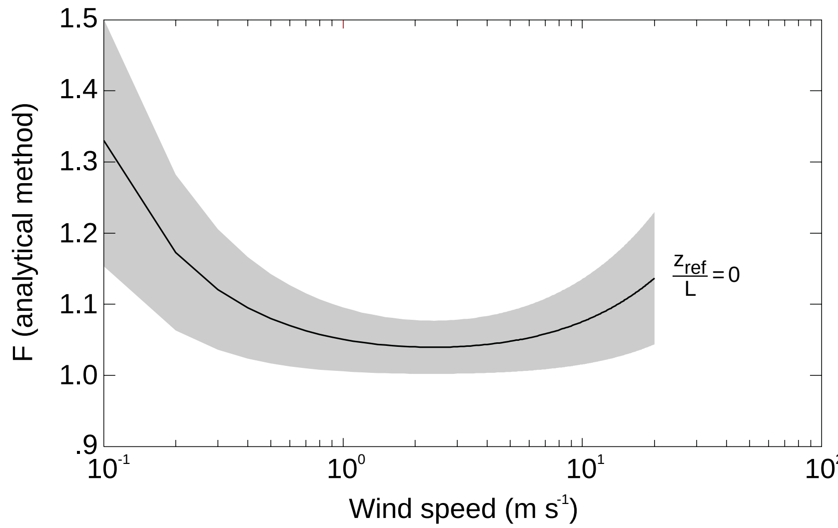

Figure 4.8. The correction factor, F, as a function of wind speed for the GLEES CO_2 covariance measurement as estimated by the analytical method of M21 (dark solid line) and its inherent range of variablity as predicted by Equation 4.2 (shaded area). The factor C used with Equation 4.2 to account for the variable (random) departures from smooth cospectral shape is 1.2, which is the same as with the GLEES open path sensor.

published (of which we are aware) that discusses $\Delta\tau_1$, which we would suggest be used to estimate $\Delta\tau_e$. However, we can easily imagine that $\Delta\tau_1$ can exceed the value of 0.025 s we use in this study.

3.7 Discussion and caveats concerning low frequencies

One of the advantages of the analytical method is the ability to estimate the high and low frequency portions of the correction factors separately. Rewriting Equation 4.4 using the b and p notation yields $F = [1 + 1/b][1 + p]$; where $\alpha = 1$ is assumed for simplicity. The high frequency correction factor is expressed by the p term, $[1 + p]$, while the low frequency portion is $[1 + 1/b]$. Table 4.3 (using η'_x from Table 4.1) lists these two terms for the GLEES covariance data and the simulated closed path CO_2 data. For the open path covariances both corrections are small; however, the low frequency portion tends to be slightly larger than the high frequency portion. In the case of the closed path CO_2 system the high frequency portion is by far the dominant term, which indicates the influence of the relatively longer high frequency time constant, τ_e, for closed path system than for the open path.

Table 4.3. Simplified (and approximate) high and flow frequency correction factors for the GLEES eddy covariance system estimated with M21's analytical method. The $(1+p)$ factor is for high frequency effects and the $(1+1/b)$ factor is for low frequency effects. Wind speeds are assumed to be greater than 1 $\mathrm{m\,s^{-1}}$.

Covariance	$(1+p)$	$(1+\frac{1}{b})$
$\overline{p'w'}$	1.04	1.01-1.06
$\overline{u'w'}$	1.00-1.01	1.00-1.05
$\overline{w'T_v'}$	1.00-1.01	1.00-1.03
$\overline{w'\rho_v'}$	1.01	1.00-1.04
$\overline{w'c'}$ (open)	1.01	1.00-1.03
$\overline{w'c'}$ (closed)	1.02-1.13	1.00-1.03

Nevertheless, in essence, both high and low frequency correction factors are based on extrapolations into regions of the cospectra where there are no direct observations. In the case of the high frequency corrections, this extrapolation is probably quite trustworthy because the -7/3 decay law is theoretically sound and has been observationally verified in many studies. But, considerably less is known about the very low frequency portion of the cospectra. For any sampling period, T_b, there is no observationally based information on low frequencies within the spectral band $[0,\frac{1}{T_b}]$. Therefore, by including the high pass filters (block averaging filters, etc.) in Equation 4.1 and integrating over the whole spectral waveband $[0,\infty]$ we implicitly assume that the observed turbulence cospectra extends smoothly and continuously into the unobserved portion of the cospectra. This assumption will not be true for all atmospheric conditions, like those that might occur during convective conditions or when other large scale planetary boundary layer processes are active at the time of the measurements. Under these conditions, the low frequency correction factor, $[1 + 1/b]$, will likely misrepresent the true correction factor.

At GLEES during the wintertime such large scale planetary boundary layer effects do not seem to be significant. For example, Figure 4.9 is a ogive computed from one of the 180 half hourly periods for the temperature covariance $\overline{w'T_v'}$. This particular ogive indicates that virtually all the half hourly cospectral power is contained in motions with periods shorter than about 5.5 minutes because the because the cumulative cospectral power has reached a relatively stable maximum at $3(10^{-3})$ Hz. We should note here that this particular example is an extreme case. Other ogives (not shown) indicate that motions somewhat longer than 30 minutes can contribute to half hourly at GLEES during the win-

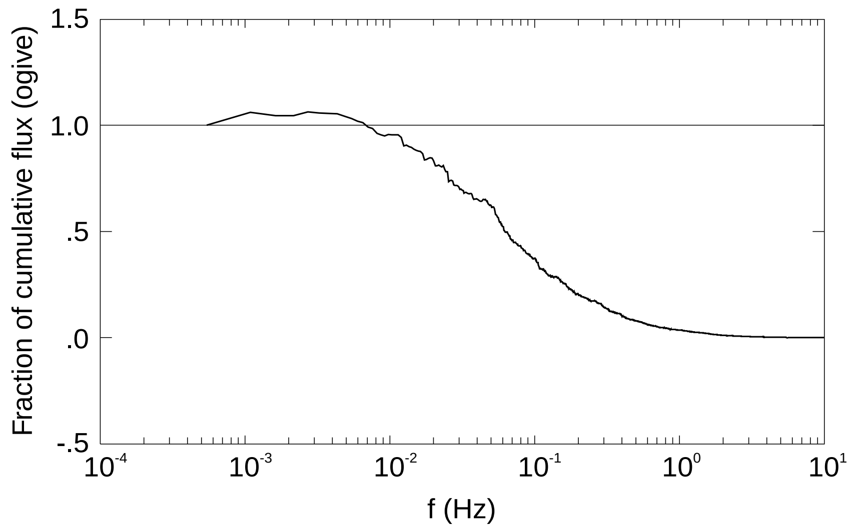

Figure 4.9. An ogive calculated from the unsmoothed FFT cospectrum for the temperature covariance $\overline{w'T_v'}$. These data were obtained at 6:30 am MST January 2, 2001 at the GLEES. Neutral atmospheric stability is assumed. This example indicates that virtually all cospectral power is located in atmospheric motions with periods less than about 5.5 minutes. Other examples (not shown) show contributions from longer period motions. The 1.0 line is highlighted.

tertime. However, we also performed other tests on the data by concatenating two half hourly time series to form a single hour time series and by subsampling and concatenating four half hourly time series to form a two hour time series. We could find no evidence of any long period, low frequency, flux contributions. Of course, this result should not be unexpected because high elevation, wintertime, high-wind, high-turbulence conditions are not particularly good candidates for low frequency planetary boundary layer motions. But when conditions are more conducive these slow large scale motions will contribute to the fluxes (Sakai et al. 2001; Finnigan et al. 2003). At present there is no single agreed-upon well defined method for correcting fluxes for these low frequency contributions. Consequently, the spectral transfer method as it is posed by Equations 4.1 and 4.2 should not be understood as compensating for all flux loss due to undersampling the low frequency planetary boundary layer motions. Issues concerning the influence of these types of motions on measured fluxes is discussed in Chapter 5 of this volume.

3.8 Summary

This study has developed a method of estimating the uncertainty in any measured covariance that is spectrally corrected by the transfer function method. It includes the effects of the (flux-averaging) period-to-period variability in (i) the frequency-weighted cospectral peak, f_x or η'_x, (ii) the random departure of measured cospectra from a smooth shape (encapsuled by the parameter C of Equation 4.7), (iii) the broadness of the frequency-weighted cospectra (μ or α), and (iv) some of the possible uncertainties in the effective time constant of an eddy covariance system, τ_e. This model, summarized by Equation 4.7, was calibrated mostly using cospectral data from one particular AmeriFlux site (GLEES), but also included comparisons with similar data from Kaimal et al. (1972) and an Euroflux site (Griffin forest). Conclusions reached in this study are

- The uncertainty associated with variability in the cospectral broadness is constant, i. e., $\Delta\alpha = 0.2$.

- It is reasonable to simplify Equation 4.7 by approximating relative uncertainty in f_x, i. e., $\Delta f_x/f_x$, by 0.4 or 0.5; where Δf_x is a measure of the inherent variability in f_x. The value of 0.4 is the upper bound of values found at GLEES (Table 4.1) and 0.5 is a value more representative of the Griffin forest site (Table 4.2). This simplification eliminates the need to evaluate Δf_x directly.

- Spectral corrections and their associated uncertainties are likely to be site specific because the nondimensional frequency, $\eta'_x = f_x(z_{ref} - d)/u$, was shown to be site specific in this study. In fact, this study has shown that η'_x varies significantly between the flat terrain site of Kaimal et al. (1972) and the micrometeorologically complex forested sites of GLEES and Griffin forest. Therefore, there is no a priori reason to assume that the values for nondimensional frequency, η'_x, developed in this study or by Kaimal et al. (1972) apply universally. In turn this suggests that to find any truly universal cospectral shape will require a different turbulent time scale than $(z_{ref} - d)/u$.

- Equation 4.7 uses a value of 1.2 for the parameter C, which seems to be reasonable for both open and closed path CO_2 systems. However, we did not emulate all possible or observed eddy covariance systems, so it is conceivable that C could be somewhat different for other eddy covariance systems. Thus there may remain a need to calibrate Equation 4.7 at more eddy covariance sites.

- The uncertainty in spectral correction, F, estimated with the transfer function method, ΔF, increases as F increases and decreases with decreasing F. Careful attention to minimizing separation distances and instrument time constants should help keep high frequency losses small so that F and ΔF are small. In this case the high frequency correction factors should be relatively independent of cospectral shape, lack of cospectral smoothness, and inherent variability.

- The spectral losses at low frequencies on the other hand are not so much instrument related as they are related to the length of the sampling period and the nature of the low frequency atmospheric motions present during a sampling period. Because so little is known about the nature of these low frequency atmospheric motions (1-4 hours) it is difficult to make specific recommendations for reducing this undersampling error. However, in general, as the measurement height decreases the low frequency content of any measured flux should also decrease, which will reduce the problem somewhat. Unfortunately, this improvement will be offset by increasing high frequency content in the fluxes.

- Present results indicate that further research is needed into the low frequency (1-4 hour) components of eddy covariance fluxes and in the nature of the differences in the frequency-weighted cospectral peaks, η'_x and f_x, between different sites.

References

Aubinet, M., Chermanne, B., Vandenhaute, M., Longdoz, B., Yernaux, M., Laitat, E.: 2001, 'Long term carbon dioxide exchange above a mixed forest in the Belgian Ardennes', *Agric. For. Meteorol.* **108**, 293-315.

Auble, D. L., Meyers, T. P.: 1992, 'An open path, fast response infrared absorption gas analyzer for H_2O and CO_2', *Bound.-Layer Meteorol.* **59**, 243-256.

Aydin, I.: 1998, 'Evaluation of fluctuating pressure measured with connection tubes', *J. Hydraulic Engineering*, **124**, 413-418.

Busch, N. E.: 1973, 'Turbulent transfer in the atmospheric surface layer', In: (Ed.) Haugen, DA, *Workshop on Micrometeorology*, American Meteorological Society, Boston, 1-28.

Coleman, H. W., Steele, W. G.: 1999, *Experimentation and Uncertainty Analysis for Engineers*. John Wiley, New York, 275 pp.

Cook, R. K., Bedard, A. J.: 1971, 'On the measurement of infrasound', *Geophysical Journal Royal Astronomical Society* **26**, 5-11.

Finnigan, J. J., Clement, R., Mahli, Y., Leuning, R., Cleugh, H.: A. 2003, 'A re-evaluation of long-term flux measurement techniques: Part 1. Averaging and coordinate rotation', *Bound.-Layer Meteorol.* **107**, 1-48.

Goulden, M. L., Daube, B. C., Fan, S.-M., Sutton, D. J., Bazzaz, A., Munger, J. W., Wofsy, S. C.: 1997, 'Physiological response of a black spruce forest to weather', *J. Geophys. Res.* **102**, 28,987-28,996.

Gurvich, A. S.: 1962, 'The pulsation spectra of the vertical component of the wind velocity and their relations to micrometeorological conditions', *Izvestiya Atmospheric Oceanic Physics* **4**, 101-136.

Hicks, B. B.: 1972, 'Propellor anemometers as sensors of atmospheric turbulence', *Bound.-Layer Meteorol.* **3**, 214-228.

Hicks, B. B., McMillen, R. T.: 1988, 'On the measurement of dry deposition using imperfect sensors and in non-ideal terrain', *Bound.-Layer Meteorol.*, **42**, 79-84.

Højstrup, J.: 1993, 'A statistical data screening procedure', *Measurement Science Technology* **4**, 153-157.

Holman, J. P.: 2001, *Experimental Methods for Engineers.* 7^{th} Edition. McGraw-Hill, Boston, MA, 698 pp.

Horst, T. W.: 1973, 'Spectral transfer functions for a three-component sonic anemometer', *J. Appl. Meteorol.* **12**, 1072-1075.

Horst, T. W.: 1997, 'A simple formula for attenuation of eddy fluxes measured with first-order-response scalar sensors', *Bound.-Layer Meteorol.* **82**, 219-233.

Horst, T. W.: 2000, 'On frequency response corrections for eddy covariance flux measurements', *Bound.-Layer Meteorol.* **94**, 517-520.

Horst, T. W., Oncley, S. P., Semmer, S. R.: 1997, 'Measurement of water vapor fluxes using capacitance RH sensors and cospectral similarity', In: *12th Symposium on Boundary Layers and Turbulence*, American Meteorological Society, Boston, 360-361.

Iberall, A. S.: 1950, 'Attenuation of oscillatory pressures in instrument lines', *Journal Research National Bureau Standards* **45**, 85-108.

Kaimal, J. C., Clifford, S. F., Lataitis, R. J.: 1989, 'Effect of finite sampling on atmospheric spectra', *Bound.-Layer Meteorol.* **47**, 337-347.

Kaimal, J. C., Finnigan, J. J.: 1994, *Atmospheric Boundary Layer Flows - Their Structure and Measurement.* Oxford University Press, New York, NY, 289 pp.

Kaimal, J. C., Kristensen, L.: 1991, 'Time series tapering for short data samples', *Bound.-Layer Meteorol.* **57**, 187-194.

Kaimal, J. C., Wyngaard, J. C., Haugen, D. A.: 1968, 'Spectral characteristics of surface-layer turbulence', *Quart. J. R. Meteorol. Soc.* **98**, 563-589.

Kaimal, J. C., Wyngaard, J. C., Izumi, Y., Coté, O. R.: 1972, 'Spectral characteristics of surface-layer turbulence', *Quart. J. R. Meteorol. Soc.* **98**, 563-589.

Katul, G. G., Hsieh, C. I.: 1999,'A note on the flux-variance similarity relationship for heat and water vapor in the unstable atmospheric surface layer', *Bound.-Layer Meteorol.* **90**, 327-338.

Koprov, B. M., Sokolov, D. Y.: 1973, 'Spatial correlation functions of velocity and temperature components in the surface layer of the atmosphere', *Izvestiya Atmospheric Oceanic Physics* **4**, 178-182.

Kristensen, L., Mann, J., Oncley, S. P., Wyngaard, J. C.: 1997, 'How close is close enough when measuring scalar fluxes with displaced sensors', *J. Atmos. Oceanic Technol.* **14**, 814-821.

Laubach, J., McNaughton, K. G.: 1999, 'A spectrum-independent procedure for correcting eddy fluxes measured with separated sensors', *Bound.-Layer Meteorol.* **89**, 445-467.

Laubach, J., Teichmann, U.: 1996, 'Measuring energy budget components by eddy correlation: Data corrections and application over low vegetation', *Beiträge Physik Atmosphäre*, **69**, 307-320.

Lee, X., Black, T. A.: 1994, 'Relating eddy correlation sensible heat flux to horizontal sensor separation in the unstable atmospheric surface layer', *J. Geophys. Res.* **99**, 18,545-18,553.

Massman, W. J.: 1991, 'The attenuation of concentration fluctuations in turbulent flow through a tube', *J. Geophys. Res.* **96**, 15,269-15,273.

Massman, W. J.,: 2000, 'A simple method for estimating frequency response corrections for eddy covariance systems', *Agric. For. Meteorol.* **104**, 185-198.

Massman, W. J.: 2001, 'Reply to comment by Rannik on "A simple method for estimating frequency response corrections for eddy covariance systems"', *Agric. For. Meteorol.* **107**, 247-251.

Massman, W. J., Lee, X.: 2002, 'Eddy covariance flux corrections and uncertainties in long-term studies of carbon and energy exchanges', *Agric. For. Meteorol.* **113**, 121-144.

Mestayer, P. G., Larsen, S. E., Fairall, C. W., Edson, J. B.: 1990, 'Turbulence sensor dynamic calibration using real-time spectral computations', *J. Atmos. Oceanic Technol.* **7**, 841-851.

Moncrieff, J., Massheder, J., Verhoef, A., Elbers, J., Heusinkveld, B., Scott, S. L., DeBruin, H. A. R., Kabat, P. , Soegaard, H., Jarvis, P.: 1997, 'A system to measure Surface fluxes of momentum, sensible heat, water vapour and carbon dioxide', *J. Hydrol.* **188**, 589-611.

Moore, C. J.: 1986, 'Frequency response corrections for eddy correlation systems', *Bound.-Layer Meteorol.* **37**, 17-35.

Nishiyama, R. T., Bedard, A. J.: 1991, 'A "Quad-Disc" static pressure probe for measurement in adverse atmospheres: With a comparative review of static pressure probe designs', *Review Scientific Instruments* **62**, 2193-2204.

Press, W. H., Teutkolsky, S. A., Vetterling, W. T., Flannery, B. P.: 1992, *Numerical Recipes*, Second Edition, Cambridge University Press.

Rannik, Ü.: 2001, 'A comment on the paper by W.J. Massman "A simple method for estimating frequency response corrections for eddy covariance systems"' *Agric. For. Meteorol.* **107**, 241-245.

Rannik, Ü., Vesala, T.: 1999, 'Autoregressive filtering versus linear detrending in estimation of fluxes by the eddy covariance method', *Bound.-Layer Meteorol.* **91**, 259-280.

Sakai, R. K., Fitzjarrald, D. R., Moore, K. E.: 2001, 'Importance of low-frequency contributions to eddy fluxes observed over rough surfaces', *J. Appl. Meteorol.* **40**, 2178-2192.

Scarborough, J. B.: 1966, *Numerical Mathematical Analysis*, 6th Edition, The Johns Hopkins Press, Baltimore.

Silverman, B. A.: 1968, 'The effect of spatial averaging on spectrum estimation' *J. Appl. Meteorol.* **7**, 168-172.

Spanier, J., Oldham, K. B.: 1987, *An Atlas of Functions*, Springer-Verlag, Berlin, 700 pp.

Verma, S. B., Ullman, F. G., Billesbach, D., Clement, R. J., Kim, J.: 1992, 'Eddy correlation measurements on methane flux in a northern peatland ecosystem' *Bound.-Layer Meteorol.* **58**, 289-304.

Vickers, D., Mahrt, L.: 1997, 'Quality control and flux sampling problems for tower and aircraft data', *J. Atmos. Oceanic Technol.* **14**, 512-526.

Villalobos, F. J.: 1996, 'Correction to eddy covariance water vapor flux using additional measurements of temperature', *Agric. For. Meteorol.* **88**, 77-83.

Webb, E. K., Pearman, G. I., Leuning, R.: 1980, 'Correction of flux measurements for density effects due to heat and water vapor transfer', *Quart. J. R. Meteorol. Soc.* **106**, 85-106.

Wilczak, J. M., Oncley, S. P., Stage, S. A.: 2001, 'Sonic anemometer tilt correction algorithms', *Bound.-Layer Meteorol.* **99**, 127-150.

Wyngaard, J. C.: 1971, 'Spatial resolution of a resistance wire temperature sensor', *Physics of Fluids* **14**, 2052-2054.

Wyngaard, J. C., Siegel, A., Wilczak, J. M.: 1994, 'On the response of a turbulent-pressure probe and the measurement of pressure transport', *Bound.-Layer Meteorol.* **69**, 379-396.